Matched Quantization and Band Separation in a Direct Sampling Dual Band GNSS Receiver for Civil Aviation

Antoine Blais, Christophe Macabiau, Olivier Julien

Matched Quantization and Band Separation in a Direct Sampling Dual Band GNSS Receiver for Civil Aviation

Antoine BLAIS, Christophe MACABIAU, and Olivier JULIEN

École Nationale de l'Aviation Civile

Biographies

Antoine Blais graduated as an Engineer from the ENAC, the French Civil Aviation University, in 1993 (Electronics specialization). From 1993 till 2001, he worked as an engineer for the French Civil Aviation Authority. He returned to the ENAC in 2001, where he obtained a Master of Science in Signal, Image and Acoustics from the Institut National Polytechnique from Toulouse in 2003. He is currently a teacher in Signal Processing and Signal Transmission fields and also an ENAC Engineer Studies Supervisor. Moreover Antoine Blais started a PhD thesis in the Telecom lab of the ENAC under the supervision of Christophe Macabiau and Olivier Julien. His topic of study is "Feasibility of Direct Sampling SDR GNSS Receivers for Civil Aviation".

Dr. Christophe Macabiau graduated as an electronics engineer in 1992 from the ENAC in Toulouse, France. Since 1994, he has been working on the application of satellite navigation techniques to civil aviation. He received his Ph.D in 1997 and has been in charge of the signal processing lab of ENAC since 2000. He is now the head of the Telecom Lab at ENAC.

Olivier Julien is the head of the SIGnal processing and NAVigation (SIGNAV) research group of the TELECOM lab of ENAC (French Civil Aviation University), Toulouse, France. His research interests are GNSS receiver design, GNSS multipath and interference mitigation and GNSS interoperability. He received his engineer degree in 2001 in digital communications from ENAC and his PhD in 2005 from the Department of Geomatics Engineering of the University of Calgary, Canada.

Abstract

This paper studies the application of the Direct Sampling technique to GNSS receivers dedicated to Civil Aviation usage. After a description of the specific spectral environment to be withstood by such receivers, two previously proposed architectures are reviewed. In the first one the E5a/L5 band and the E1/L1 band are sampled by a unique ADC, providing full coherency between bands. In the second architecture each band is sampled separately. The minimum sampling frequencies are also recalled for each architecture. The quantization process is then analyzed and the required number of bits assessed in each case, taking into account the full range of the input signal, possibly tainted by strong interference. The high values found motivate the study of two low complexity non-linear functions dedicated to dynamic compression at the output of the ADCs, in order to decrease the computation workload of the following signal processing tasks. Finally the filters needed to separate the E5a/L5 and E1/L1 bands in the the first coherent sampling architecture are specified and the induced computation workload is estimated.

1 Introduction

Due to software's superior adaptability over hardware, software is being used increasingly often in new receiver designs, and especially in GNSS receivers. Each increase in computing capacity or advance in Analog to Digital Converter (ADC) technology brings the ADC closer to the antenna. In fact, analog correlators now no longer exist. Next to disappear will undoubtedly be Intermediate Frequency (IF) translation stages as sampling frequencies high enough to allow RF Direct Sampling (DS) are already available on the market. Finally the analog Automatic Gain Control (AGC) will give way to a digital one in light of the upcoming availability of a sufficient number of quantification bits required to linearly quantize the full range of input signal. The complete Software Defined Radio (SDR) seems to be in view: an antenna, an ADC and a processor. However,

even if technology rapidly keeps its promises, and permits such a design for mass market GNSS receivers for which extreme operational robustness is not necessarily a key point, additional difficulties are expected for more demanding applications. In particular, for Civil Aviation purposes, GNSS receivers must meet the stringent requirements found in standards, for instance, the Galileo (EUROCAE, 2010) and GPS (RTCA, 2009), (RTCA, 2008b) or (RTCA, 2006) Minimum Operational Performance Specifications (MOPS) documents. Among the most severe requirements, are the interference levels the receiver must withstand without degradation of its operational capability. As an illustration, it is noted that at the input of the Civil Aviation receiver the dynamic range between useful signals and Carrier Wave (CW) interference can reach 50 dB for the L1/E1 band. For the L5/E5a band, the situation is no better because this dynamic range, with the cumulation of in-band Distance Measuring Equipment (DME) ground emissions, can be as high as 30 dB. Taking these requirements as design specifications, we proposed in previous papers (Bla, 2011) and (Bla, 2012) two different SDR DS GNSS receiver architectures for Civil Aviation, using both L5/E5 and L1/E1 bands. We targeted a final objective of "neither AGC nor IF". The first solution has one global channel leading to one ADC digitizing the input signal to provide as output a signal including both L5/E5 and L1/E1 bands very close to each other. The second solution has one channel per band each ending with an ADC. The aim of this article is to extend the study of DS SDR architectures for Civil Aviation GNSS receivers. More specifically we address two points. The first relates to the high binary throughput, which results from the digitization process and is necessary to reflect all interference levels. We propose methods to minimize this throughput in order to lower the workload of signal processing tasks, preserving the signal. The second point we study is specific to the first proposed architecture. It consists in determining a process to digitally separate L5/E5a and L1/E1 bands, subsampled in one block with the lowest sampling frequency and so closely aliased, whilst keeping out-of-band interference at a low power. In the first part of this paper we present the context of Civil Aviation GNSS receivers, focusing on requirements regarding robustness against interference. We display interference masks at the antenna port specified in the MOPS. They define the maximal power of the interfering signals below which all the minimum performance requirements must be met. Taking into account the minimum required selectivity of the on-board active antenna we are then able to deduce the second level interference masks, at the receiver input. In a second section we review the two Direct Sampling architectures we previously elaborated from these second level masks, identifying the essential minimal RF hardware element and recalling the minimum values of sampling frequencies we calculated. The third part is dedicated to the calculation of the number of quantification bits required to linearly quantize the input signal over the range defined by the second level masks. We then present in a fourth section methods to minimize the bit rate immediately after the ADC. On average we would expect good data economy because most of the time the interference threat will be absent. In a fifth and last section we detail the digital separation process of L5/E5a and L1/E1 bands in the architecture where they are sampled together. That is we have to design sharp digital filters which not only select each band but also protect it from possible interference present in the other band.

2 GNSS Receivers for Civil Aviation

The interference threat a Civil Aviation GNSS receiver can face has been quantified by standardization committees and is summarized in three documents, (RTCA, 2008a) and (RTCA, 2004) for respectively the L1 and L5 GPS signals, and (EUROCAE, 2010) for both E1 and E5 Open Service Galileo signals. Considering that, from the spectral standpoint, E1 band equals L1 band and E5 band includes L5 band and that the MOPS for Airborne Open Service Galileo Satellite Receiving Equipment document (EUROCAE, 2010) is the only one which considers a dual band receiver in a unified way, (EUROCAE, 2010) will be used as a single reference in the rest of this paper. Anyway the levels of interference described in (RTCA, 2008a), (RTCA, 2004) and (EUROCAE, 2010) are comparable.

The requirements about robustness against interferences found in (EUROCAE, 2010) are defined at receiver antenna port. This port, as well as the receiver input are defined graphically in figure 1. These requirements can be represented, as proposed in figure 2, as masks which define the maximal power of the interfering signals below which all the minimum performance required for the receiver shall be achieved. The high dynamic range, from +30 dBm to -118 dBm, the receiver has to sustain can immediately be noted.

2.1 Interference Masks at Antenna Port

The receiver useful signal bands can also implicitly be defined from the figure 2 as the frequency ranges where the mask is at its lower values, that is $B_{E5a} = [1166.45, 1186.45]$MHz for E5a/L5 and $B_{E1} = [1565.42, 1585.42]$MHz for E1/L1.

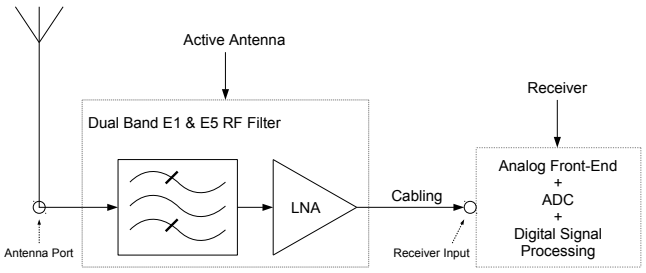

Figure 1. Receiver ports definition

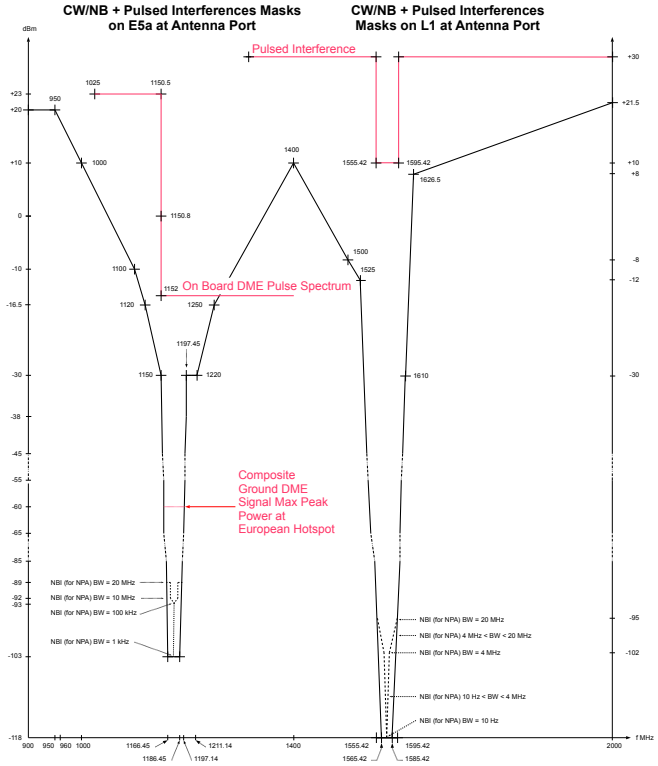

Figure 2. Interference masks at antenna port

2.2 Antenna Selectivity

Standards also specify the requirements for active antenna to be used on board. The corresponding required minimum preamplifier selectivity in both E1 and E5 bands are represented in figure 3 extracted from (EUROCAE, 2010).

2.3 CW Interference Masks at Receiver Input

Using the minimum preamplifier selectivity curves it is possible to deduce the maximum interference levels at the receiver input as drawn in figure 4 if input interference is at the mask level. Narrow Band (NB) interference mask is not represented because, as it will be shown later on, Carrier Wave mask has higher power levels at frequencies of interest. Regarding Pulsed interferences with power above CW mask (which is, out-

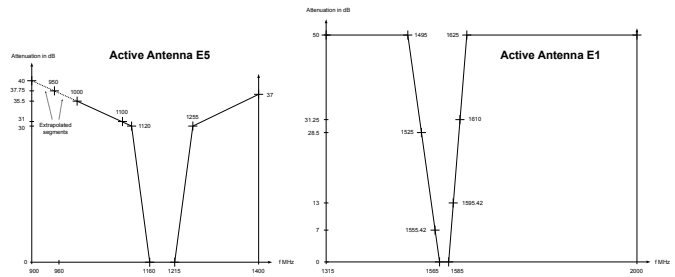

Figure 3. Minimum required selectivity of the active antenna

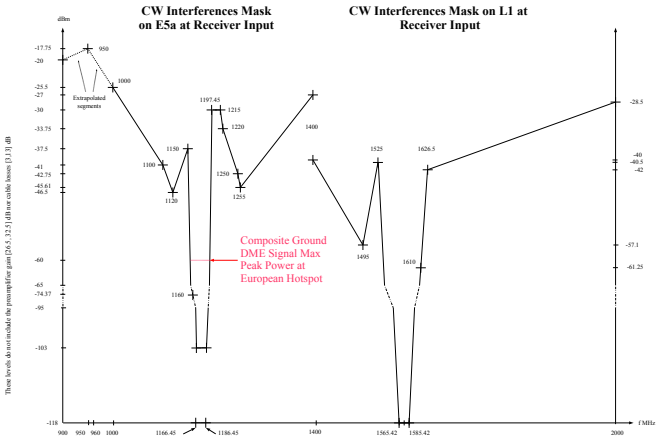

Figure 4. CW interference mask at receiver input

of-band, around 5 dB under the compression point of the preamplifier also specified in (EUROCAE, 2010)), they lead to saturation with unpredictable spectral effects. So we also propose to not consider their spectral content in the design of the RF Front-End and that is why they are not on the drawing as well.

3 Proposed Direct Sampling Architectures

Direct Sampling architectures for multi-band GNSS receivers have already been studied in some other publications as (Psi, 2003), (Alonso et al., 2008) and (Parada et al., 2009), but our approach includes the interference threat and goes further into hardware simplification by removing the need of AGC. That is, ideally, the structure of this kind of receiver could be as simple as the one represented in figure 5.

Sampling directly the spectral content represented in figure 4 requires a sampling frequency greater or equal to the Shannon's Frequency, that is at least 2 times 2GHz here i.e $4GS/s$, which is huge in comparison to the total bandwidth of the useful signals, 20MHz for each bands i.e. a total of 40MHz.

That is why undersampling was the chosen technique in (Bla, 2011) and (Bla, 2012) to propose two different architectures for a Direct Sampling Software

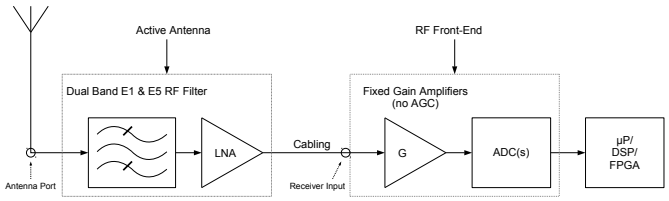

Figure 5. Ideal Direct Sampling GNSS receiver for Civil Aviation

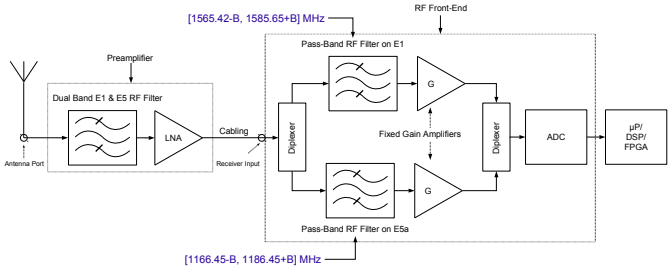

Figure 6. Coherent Direct Sampling

Defined Radio GNSS receiver. In the first architecture, called Coherent Sampling, the two bands E5/L5 and E1/L1 are sampled by the same unique ADC, by opposition to the second architecture where each band is sampled by its own ADC.

3.1 Coherent Sampling

In this first architecture, sketched in figure 6, both bands are digitized at the same time because only one ADC is used. This provides a perfect coherency between the two, as long as the differences in their different RF paths are known and compensated. In particular the sampling jitter is the same on each band.

Some extra filters appear here because, as it is explained in (Bla, 2011), due to the interference threat, it is not possible to undersample the signal directly at the receiver input. Otherwise, aliasing due to the sampling operation could provoke the crushing of a useful band by a more powerful part of the interference mask. The task of the extra filters is then to attenuate the out-band mask under the in-band mask so that out-band aliasing in-band is safe.

A representation of the magnitude of the ideal transfer functions of these extra filters is given in figure 7. They were calculated so that in-band aliasing of an out-band threat is attenuated to a level of 10dB less than the minimum in-band mask, −118dBm in the E1/L1 band.

Applying these ideal transfer functions to the CW interference mask 4 at the receiver input gives the new maximum spectral content to be considered at the input of the ADC. It is drawn in figure 8.

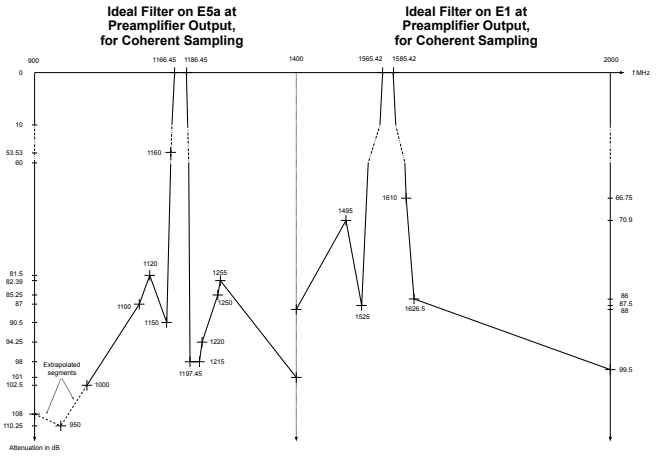

Figure 7. Magnitude of the ideal transfer functions of the extra filters needed for Coherent Sampling

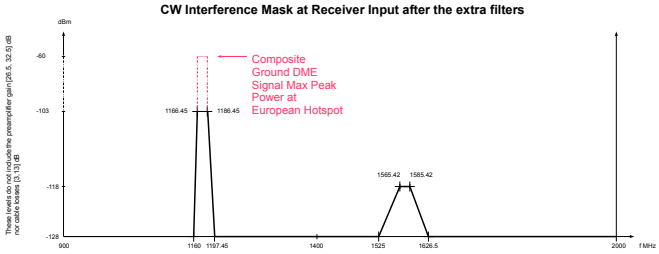

Figure 8. Maximum spectral content at the input of the ADC with Coherent Sampling

It is then possible to calculate the minimum sampling frequency which allows the aliasing of the useful bands without overlapping. If the ideal transfer functions of the extra filters could not be reached for some reason, this minimum sampling frequency was also calculated for a supplementary transition bandwidth B around each side of the useful bands. The results are presented in figure 9. Two bound values are of interest. The first is the minimum minimorum sampling frequency, 88.079MS/s, which is approximately equal to twice the total bandwidth of the useful signals. The second is the maximum supplementary transition bandwidth, 28MHz, above which there is no sampling frequency which allows to undersample the signals.

3.2 Separate Sampling

The second proposed architecture does not provide coherency, but in return relaxes the need to perfectly compensate for the different RF paths. It is represented in figure 10. Again some extra filters are needed for the same reason than with Coherent Sampling. But the required minimum selectivity is different because, as each band is sampled separately, it does not matter if during the sampling of the E5a/L5 band the E1/L1 band

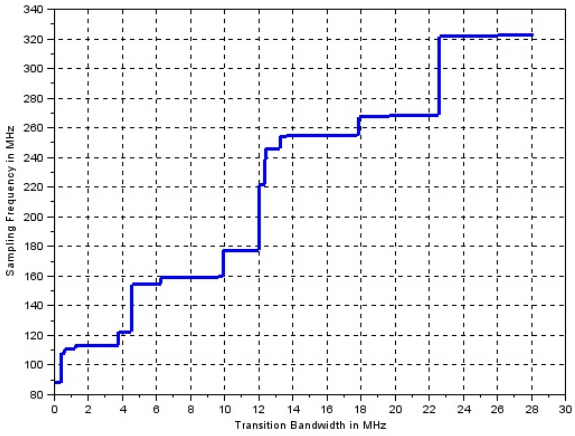

Figure 9. Minimum coherent sampling frequency vs transition bandwidth B

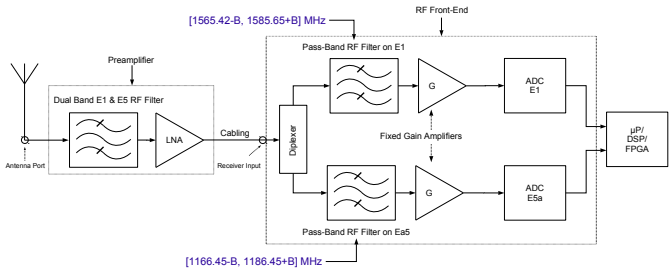

Figure 10. Separate Direct Sampling

is crushed, and vice versa.

A representation of the magnitude of the ideal transfer functions of these extra filters is given in figure 11. They were calculated, for each band, so that in-band aliasing of an out-band threat is attenuated to a level of 10 dB less than the minimum in-band mask, −103dBm in the E5a/L5 band and −118dBm in the E1/L1 band.

Applying these ideal transfer functions to the CW interference mask 4 at the receiver input gives the new maximum spectral content to be considered at the input of the ADCs. It is drawn in figure 12.

Again it is then possible to calculate the minimum sampling frequency, but for each band separately here, which allows the aliasing of the useful band without overlapping. If the ideal transfer functions of the extra filters could not be reached for some reason, this minimum sampling frequency was also calculated for a supplementary transition bandwidth B around each side of the useful band. The results are presented in figure 13. Only one bound value is of interest in this case: the minimum minimorum sampling frequency, 40.219MS/s for the E5a/L5 band and 40.137MS/s for the E1/L1

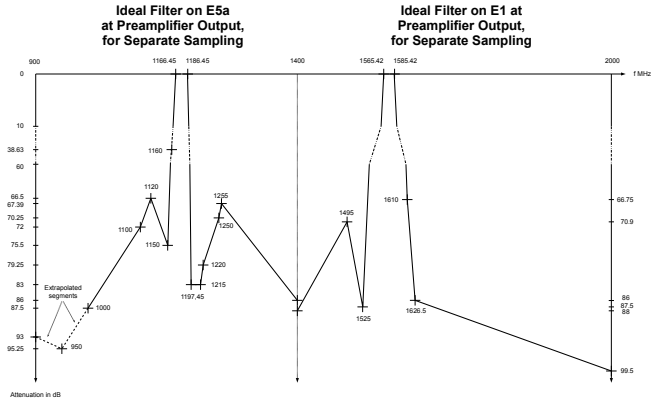

Figure 11. Magnitude of the ideal transfer functions of the extra filters needed for Separate Sampling

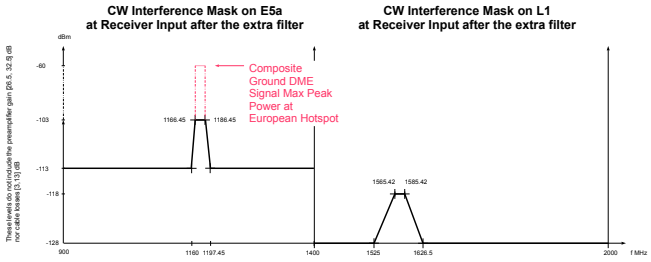

Figure 12. Maximum spectral content at the input of the ADCs with Separate Sampling

band, which is approximately equal in each case to the bandwidth of the useful signal. It is interesting to sum the two sampling frequency, which gives 80.356 MS/s, nearly the same value than in Coherent Sampling. But here the two bands are digitally separated at source, as opposed to the Coherent Sampling architecture where this separation is left to be done, as it is studied in the last part of this paper.

4 Quantization

After sampling, quantization is the second operation to address in order to completely characterize the digitization process which happens in a SDR GNSS receiver. To scale the quantization stage of the ADC(s), two reference amplitude levels must be considered.

4.1 Low Reference Amplitude Level

This level sets the minimum number of bits k required to correctly digitize the minimum system equivalent thermal noise, in which the useful signals are completely buried. Usually k is between 1 and 5.

(EUROCAE, 2010) specifies the interference masks, but also assesses the system noise through the equivalent temperature of the noise at the antenna port, $T_{sky} = 100$K and the actual cable temperature,

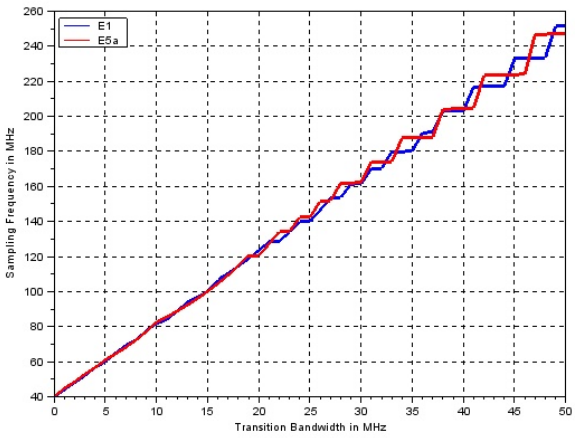

Figure 13. Minimum separate sampling frequency vs transition bandwidth B

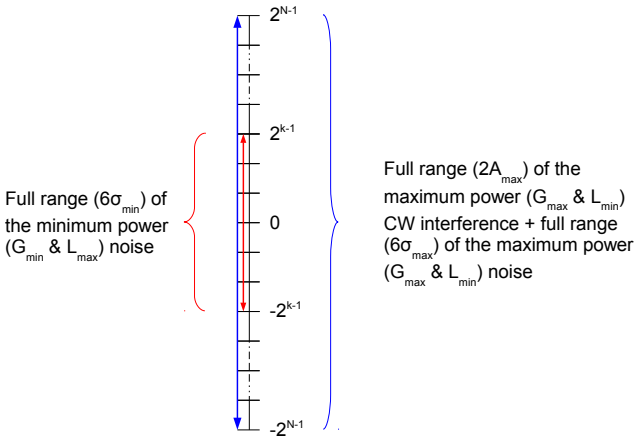

Figure 14. Dimensioning values of the quantifier

$T = T0 = 290$K. Combined to the specified preamplifier gain $G \in [26.5, 32.5]$dB, its noise factor $F = 4$dB and the cable losses $L \in [-3, -13]$dB, it gives a noise density level

$$\mathrm{N0} = kG\left(T_{sky} + (F-1)T0\right)/L + k(1-1/L)T$$

We write $\mathrm{N0} \in [\mathrm{N0}_{min}, \mathrm{N0}_{max}]$dBm/Hz at the input of the ADC(s).

As the proposed architectures aim at being *aircraft installation independent*, they must cope with the full range of preamplifier gain and cable losses. It means that k must be calculated for the lowest noise level, corresponding to $\mathrm{N0}_{min}$. Under the classical assumption that this system noise can be modeled as a gaussian random process, the pertinent value is not the Power Spectrum Density (PSD) value N0 but its standard deviation $\sigma \in [\sigma_{min}, \sigma_{max}]$. For the Coherent Sampling architecture $\sigma^2 = \mathrm{N0} \times (B_{E1} + B_{E5a}) = 2\mathrm{N0} \times B_{E1}$ at the input of the unique ADC, whereas $\sigma^2 = \mathrm{N0} \times B_{E1} = \mathrm{N0} \times B_{E5a}$) at the input of each ADC for the Separate Sampling architecture.

Writing Δ the quantifier step size and considering that the (useful signals +) maximum minimum noise amplitude is $3\sigma_{min}$ (this value is proposed as the dimensioning element because the cumulative probability for the amplitude to lie in $[-3\sigma_{min}, +3\sigma_{min}]$ is above 99%), then we have the relation

$$2^k \times \Delta \geq 6\sigma_{min}$$

4.2 High Reference Amplitude Level

This level sets the full scale of the ADC(s). It corresponds to the total number of bits N of the ADC(s). This high level is obviously a function of the interference mask at the input of the ADC(s), but also of the noise level as it is always present. Again, the proposed architectures aim at being *aircraft installation independent*. It means that this time this high reference level must be calculated with the maximum active antenna gain $G_{max} = 32.5$dB and the minimum cable losses $L_{min} = -3$dB to cover the maximum maximorum level of the signal at the input of the ADC(s). At this point we make the assumption that the CW aggression is limited to one interference at a time per band, as the tests imposed in (EUROCAE, 2010) suggest it. It means that for Coherent Sampling the maximum interference level A_M to be considered is the sum of the maximum amplitudes found in the mask for E5a/L5 on the one hand and for E1/L1 on the other, whereas for Separate Sampling it is either the maximum amplitude A_{M5a} found in the mask for E5a/L5 for the corresponding ADC or the maximum amplitude A_{M1} found in the mask for E1/L1 for the other ADC.

The high reference level is then the sum of the maximum interference level A_M, A_{M5a} or A_{M1}, multiplied by G_{max} and L_{min}, and of the highest noise level, corresponding to $\mathrm{N0}_{max}$.

Writing A_{max} the generic value for A_M, A_{M1} or A_{M5a} and considering again that the maximum maximum noise amplitude is $3\sigma_{max}$, this high reference level equals $\sqrt{G_{max}L_{min}} \times A_{max} + 3\sigma_{max}$.

A graphical representation of the dimensioning values k and N can be found in figure 14.

The following relation can then be established

$$2^N \times \Delta \geq 2\sqrt{G_{max}L_{min}} \times A_{max} + 6\sigma_{max}$$

A simple algebraic division gives the result

$$N - k \geq \log_2\left(\frac{\sqrt{G_{max}L_{min}} \times A_{max} + 3\sigma_{max}}{3\sigma_{min}}\right) \quad (1)$$

Thus, setting k, N can be calculated as a function of A_{max} only.

As it is detailed hereafter, this level A_{max} is quite dependent of the real transfer functions of the extra filters required in both proposed architectures.

4.3 Quantization with ideal filters

4.3.1 Coherent Sampling

If the extra filters used before digitization meet the minimum selectivity drawn in figure 7 then the interference mask to be considered at the input of the ADC is the one represented in figure 8. It can be read that for E5a/L5 band the maximum threat is the composite ground DME signal maximum peak power at the European hotspot, −60dBm, and that it is the floor of its CW interference mask for the E1/L1 band, −118dBm.

It can be calculated then that $N - k > 7.5$: $N = 9, 10, 11, 12, 13$ for $k = 1, 2, 3, 4, 5$.

4.3.2 Separate Sampling

If the extra filters used before digitization meet the minimum selectivity drawn in figure 11 then the interference mask to be considered at the input of the ADCs is the one represented in figure 12. It can be read that A_{M5a} corresponds also to the composite ground DME signal maximum peak power at the European hotspot, −60dBm and that A_{M1} is equal to the floor of the interference mask for the E1/L1 band, −118dBm too.

This gives

- on E5a/L5 $N - k > 2.7$: $N = 4, 5, 6, 7, 8$ for $k = 1, 2, 3, 4, 5$.
- on E1/L1 $N - k > 8.0$: $N = 9, 10, 11, 12, 13$ for $k = 1, 2, 3, 4, 5$.

4.4 Quantization after sub-optimal filters

If the extra filters are not as selective as required, they can pass the interference threat up to a very high level, depending of the width of their actual transition bandwidth.

4.4.1 Coherent Sampling

At the input of the ADC the situation can be as deteriorated as the one presented in figure 15, which corresponds to the maximum transition bandwidth $B =$ 28MHz which allows coherent undersampling.

In this worse situation, for the E5a/L5 band the maximum threat is a CW interference which can reach −30dBm at 1197.45MHz and for the E1/L1 band it is also a CW interference which can reach −57.26dBm at 1613.42MHz this time.

The new total number of bits N' of the ADC is then link to k by this relation : $N' - k > 12.5$: $N' = 18$ for $k = 5$. At most 5 bits more than with ideal filters are needed.

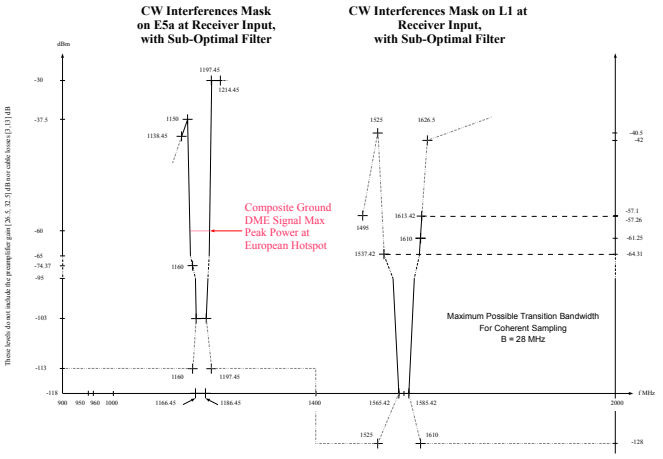

Figure 15. CW interference mask at receiver input with sub-optimal filters, Coherent Sampling

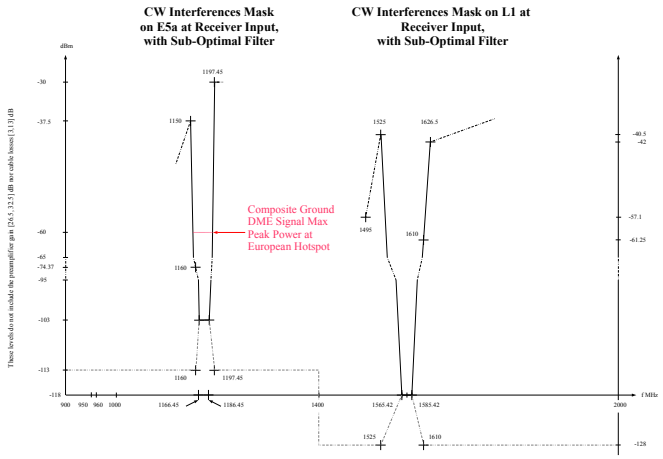

Figure 16. CW interference mask at receiver input with sub-optimal filters, Separate Sampling

4.4.2 Separate Sampling

This time the situation at the input of the ADCs can be as bad as the one presented in figure 16. It is to be noted that here a maximum transition bandwidth which allows coherent undersampling also exists, but is greater than 50MHz and so is not represented as undoubtedly the actual analog filters will exhibit a lower one. In addition we make the assumption that these analog filters will be selective enough so that we can consider the maximum threat for the E1/L1 band is a CW interference which can reach −40.5dBm at 1626.5MHz (it corresponds to a transition bandwidth greater than 40MHz). For the E5a/L5 band the maximum threat is as previously a CW interference which can reach −30dBm at 1197.45MHz. In these condi-

tions, the new total number of bits N' of each ADC is given by the relation

- for the E5a/L5 band, $N' - k > 13.4$: $N' = 19$ for $k = 5$. At most 6 bits more than with ideal filters are needed.

- for the E1/L1 band, $N' - k > 11.7$: $N' = 17$ for $k = 5$. At most 9 bits more than with ideal filters are needed.

5 Binary Throughput Reduction

After digitization, the following process should be a filtering operation dedicated to the mitigation of the interference threat. As examples in the Separate Sampling case, the minimum attenuation which should be provided by these filters, versus frequency, is given in figure 17 for the E5a/L5 band and in figure 18 for the E1/L1 band.

The attenuation is calculated from figure 16 for each band respectively, so that in-band aliasing of an out-band threat is attenuated to the minimum in-band mask level, -103dBm in the E5a/L5 band and -118dBm in the E1/L1 band.

If Finite Impulse Response (FIR) filters are to be used, figure 19 for the E5a/L5 band and figure 21 for the E1/L1 band give an estimation of the minimum order of the filter vs transition bandwidth. Figure 20 for the E5a/L5 band and figure 22 for the E1/L1 band propose an estimation of the induced calculation workload, versus transition bandwidth also.

The calculation workload is estimated here by the simple product of the filter order $\hat{M}$ and of the minimum sampling frequency, which is a function of the transition bandwidth as presented in section 3. So this estimated workload does not take into account the various optimization techniques which could be used in the actual implementation of these FIR filters. This workload can reach 2630MMAC/s for the E5a/L5 band and 4465MMAC/s for the E1/L1 band. The MAC unit corresponds to the computation of the product of two numbers and the addition of the result to an accumulator. This unit is used to quantify the performance of signal processors as for example the Analog Devices TigerSHARC ADSP-TS201S Digital Signal Processor (DSP) (AD, 2006), which can reach 4.8GMAC/s.

The following formula, from (Herrmann et al., 1973), was used to estimate the filter order

$$\hat{M} = \frac{D_\infty(\delta_p, \delta_s) - f(\delta_p, \delta_s) \cdot (\Delta f)^2}{\Delta f} + 1$$

Digital Filter Ideal Transfer Function required to compensate for the Analog Sub-Optimal Filter on E5a

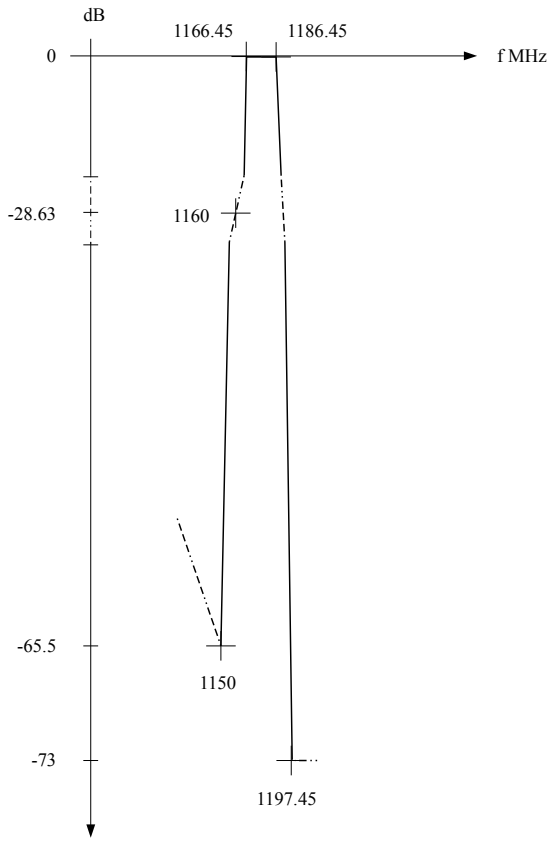

Figure 17. Minimum attenuation to be provided at the output of the ADC in the E5a/L5 band, Separate Sampling

where

$$D_\infty(\delta_p, \delta_s) = \big(0.005309(\log_{10}(\delta_p))^2 + 0.07114\log_{10}(\delta_p) - 0.4761\big) \times \log_{10}(\delta_s) - \big(0.00266(\log_{10}(\delta_p))^2 + 0.5941\log_{10}(\delta_p) + 0.4278\big) \quad (2)$$

and

$$f(\delta_p, \delta_s) = 11.012 + 0.51244\,(\log_{10}(\delta_p) - \log_{10}(\delta_s))$$

f_p is the passband edge frequency, f_s the stopband edge frequency, $\Delta f = (f_s - f_p)$ is the transition bandwidth, δ_p the passband ripple ($10\log_{10}(\delta_p) = -10$dB in the rest of this paper) and δ_s is the stopband ripple.

Considering these workload values, if we multiply them by the highest number of quantization bits, for example $N' = 17$ ($k = 5$) for the E1/L1 band, this workload can then exceed 75Gbit/s which is really important.

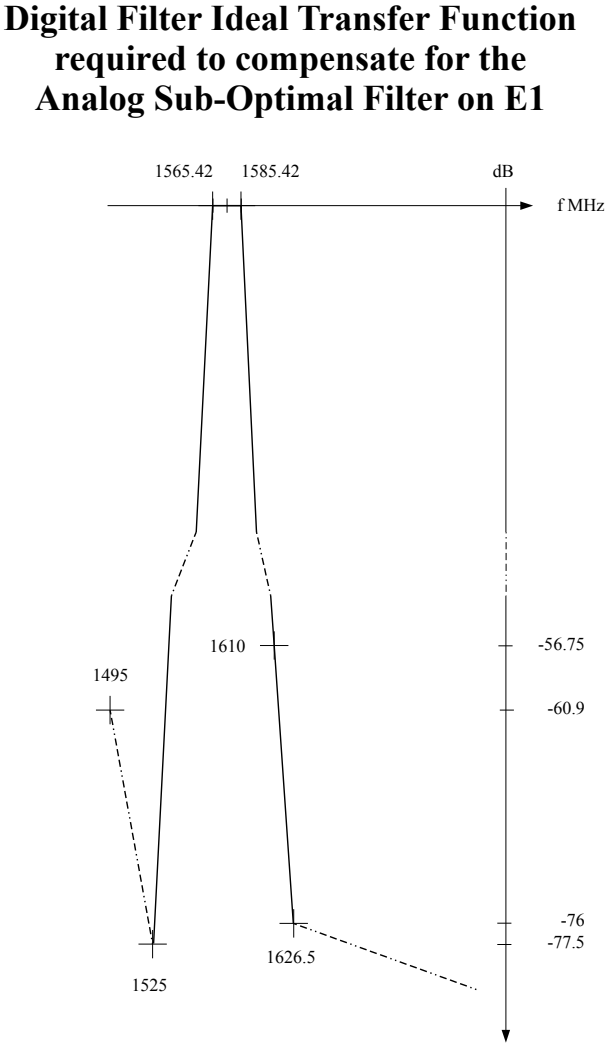

Figure 18. Minimum attenuation to be provided at the output of the ADC in the E1/L1 band, Separate Sampling

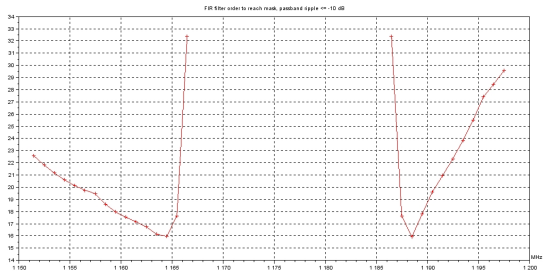

Figure 19. Minimum FIR filter order to reach the required minimum attenuation on the E5a/L5 band, Separate Sampling

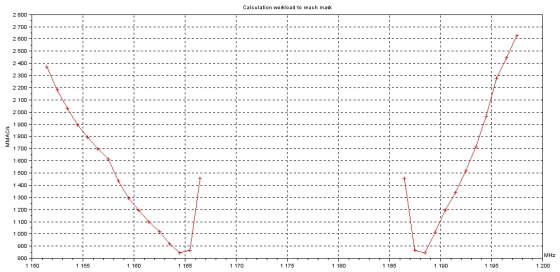

Figure 20. Estimated calculation workload on the E5a/L5 band, Separate Sampling

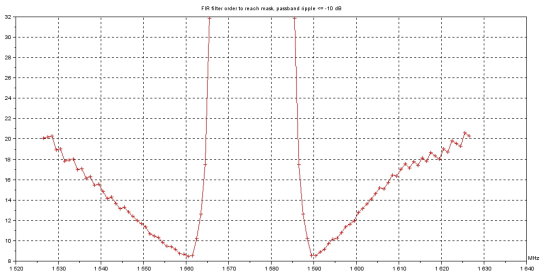

Figure 21. Minimum FIR filter order to reach the required minimum attenuation on the E1/L1 band, Separate Sampling

Therefore the question of decreasing the number of bits before the filtering operation arises.

Three methods were envisaged

- Estimation of the actual antenna gain G and of the actual cable losses L once the receiver is put in the aircraft. As (1) shows it, the lower the product $G \times L$ the lower N. For G_{min} and L_{max}, with ideal analog filters we can throw away 3 MSBs in Coherent Sampling and 2 MSBs on each channel in Separate Sampling. With sub-optimal filters only 1 MSB can be thrown away, for Coherent or Separate Sampling. As it is not a general solution

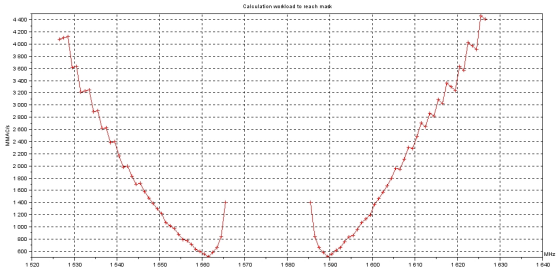

Figure 22. Estimated calculation workload on the E1/L1 band, Separate Sampling

it was not more studied.

- Digital AGC, which can keep the number of bits to the minimum needed to correctly represent the signal, as a function of the signal power at the output of the ADC(s). This solution is well known and established so it was not studied here also.
- Dynamic Reduction with non-linear functions. This is the subject of the rest of this part about binary throughput reduction.

The main idea is to compress the dynamic of the input signal (which is supposed tainted by at most one CW interference) as much as possible so that a maximum number of the MSBs, useless after this operation, can be discarded. Of course the useful signal must be preserved as much as possible, especially when there is no interference. It means that linearity must be preserved as much as possible over the full range of the useful signal. And when the interference is present, the compression of the dynamic must not produce other interferences with a level higher than the mask.

It must be noted that, as our study is limited to one CW interference, it only applies to the Separate Sampling architecture.

Two non-linear functions with low computation complexity were considered.

5.1 The Linear-then-Log Function

This function F_{ll} is represented in figure 23. Its main advantage is that it is fully linear before the corner value X0: if X0 is set greater than $3\sigma_{max}$, the dynamic compression operation is completely transparent for the useful signal in the nominal situation, i.e. when there is no interference.

The effect of this function F_{ll} on a CW parametrized by its mean power P, its frequency f_0 and its initial phase ϕ_0 (set to 0 here without loss of generality) was evaluated through the Fourier coefficients of the output signal. Indeed, as the input CW interfering signal $x(t) = sqrt2P\sin(2\pi f_0 t)$ is periodic, the output $y(t) = F_{ll}(x(t))$ is also periodic with the same period and can then be decomposed in a Fourier series

$$y(t) = \sum_{n=-\infty}^{+\infty} C_n e^{i2\pi n f_0 t}$$

where

$$C_n = f_0 \int_{-\frac{1}{2f_0}}^{\frac{1}{2f_0}} x(t) e^{-i2\pi n f_0 t} dt, n \in \mathbb{Z}$$

The single sided power spectrum of y is made of lines located at frequencies nf_0 with power $2(C_n)^2$. It must be noted that even if one harmonic is very far in frequency from the original CW interference, due to aliasing it is folded back in the sampled band.

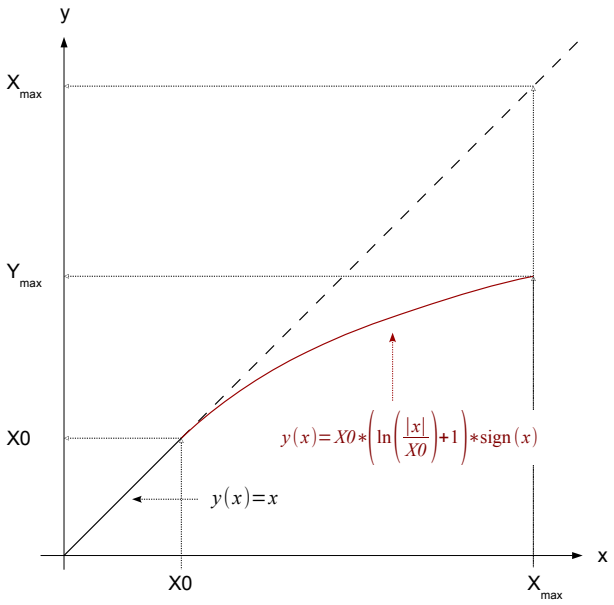

Figure 23. The linear-then-log function

To measure the performance of this linear-then-log function, the interference masks represented in figure 16 for the E5a/L5 and the E1/L1 bands were sampled and for each sample the following numerical computations were done with a CW interference of corresponding power P_{mask}

1. set X0 to $\sqrt{2P_{mask}}$,
2. calculate by numerical integration the first Fourier coefficients, the more powerful, of y,
3. test if it exists one coefficient $C_n, n > 1$ for which the power $2(C_n)^2$ exceeds the in-band mask level,
   - if yes it means that X0 is the compression limit under which dynamic reduction is dangerous,
   - if not X0 can be lowered (of 1dB in our code) and the process can loop to step 1

Doing so, X0 is calculated as low as possible (better dynamic compression) but without reinjecting in-band secondary harmonics more powerful than the interference mask.

The results are presented in figures 24, 25 and 26 for the E5a/L5 band and in figures 27, 28 and 29 for the E1/L1 band. The first plots 24 and 27 superimpose the CW interference mask at the input of F_{ll} and the corresponding power of the first harmonic $2(C_1)^2$ at the output. The second plots 25 and 28 plot directly the

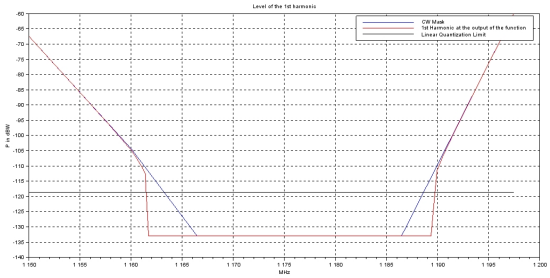

Figure 24. Compression effect of the linear-then-log function on the E5a/L5 CW interference mask

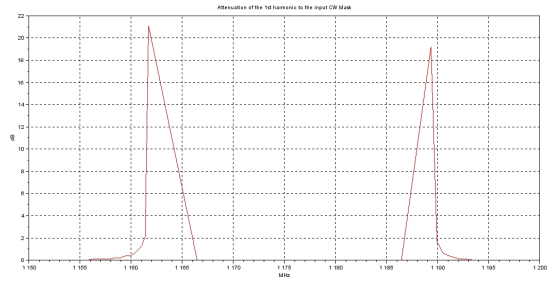

Figure 25. Attenuation provided by the linear-then-log function on the E5a/L5 CW interference mask

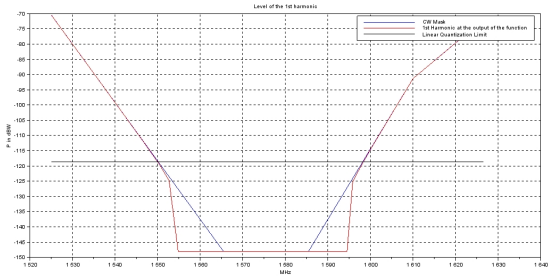

Figure 27. Compression effect of the linear-then-log function on the E1/L1 CW interference mask

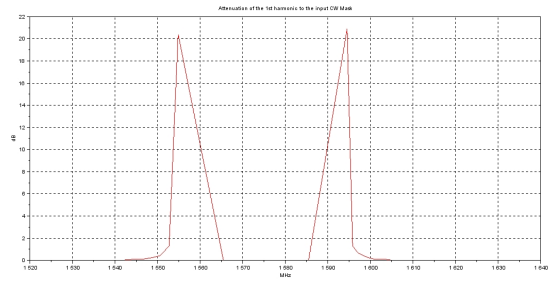

Figure 28. Attenuation provided by the linear-then-log function on the E1/L1 CW interference mask

attenuation provided by the function, $P_{mask} - 2(C_1)^2$. And the last plots 26 and 29 show the quantization bit saving offered by the dynamic compression.

From the first subplot we can define the full efficiency band of this function, the band over which after the dynamic reduction there is no more need of filtering because the level of the first harmonic lies under the in-band mask. It is equal to $[1162, 1189]$MHz for E5a/L5 and to $[1555, 1593]$MHz for E1/L1. This result by itself is interesting. and what is more the third subplot shows that in absolute a quantization bit saving up to 2 bits is possible. Unfortunately the first plot also shows that in this full efficiency band the CW interference mask is around or under the linear quantization limit which is set to 3σ as stated before: the CW level to compress is the same or smaller than the noise in which the useful signal is buried. This function F_{ll} is efficient where it can not be used. That is why a second function was considered.

5.2 The Pure Log Function

This function F_{pl} is represented in figure 30. It is fully logarithmic and it has a continuous second order derivative, by opposition to F_{ll} which has a discontinuous one at X0, property which should induce lower harmonics at the output. This is at the expense of linearity : the

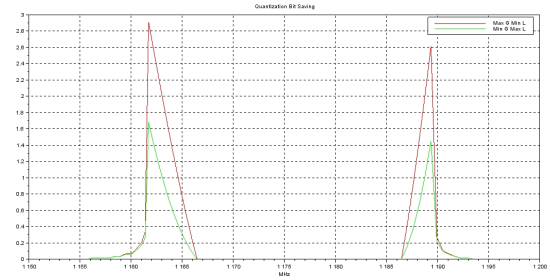

Figure 26. Quantification bit saving offered by the linear-then-log function on the E5a/L5 band

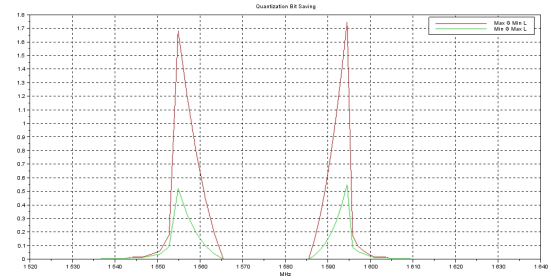

Figure 29. Quantification bit saving offered by the linear-then-log function on the E1/L1 band

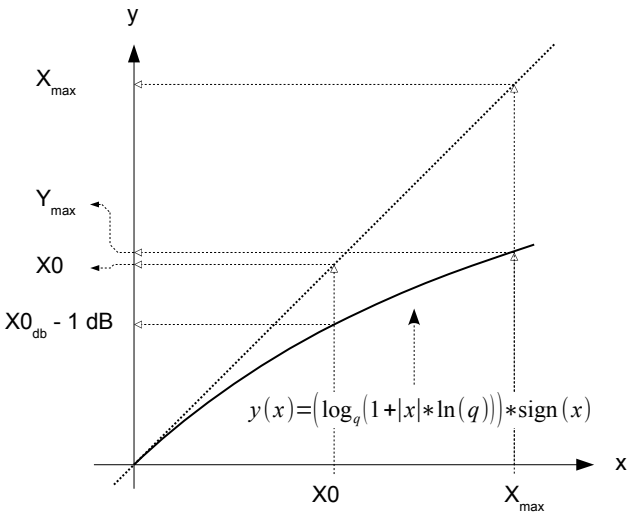

Figure 30. The pure log function

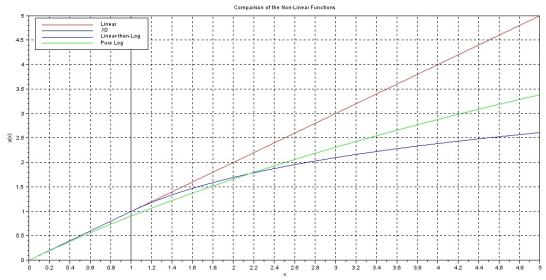

Figure 31. Comparison of the two non-linear functions

useful signal, even in the nominal situation, i.e. when there is no interference will be compressed. The corner value is defined here as the 1dB compression point. Figures 31 and 32 allows a graphical comparison between both functions. The better compression ratio of the Linear-then-Log function appears as at the same time the smoother variation of the pure log function is shown.

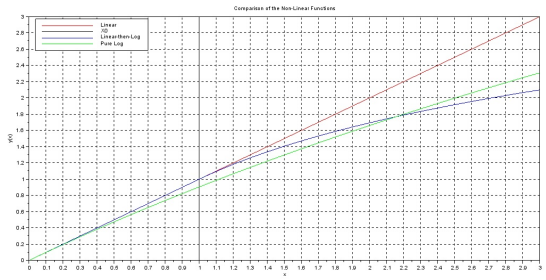

Figure 32. Comparison of the two non-linear functions, close-up

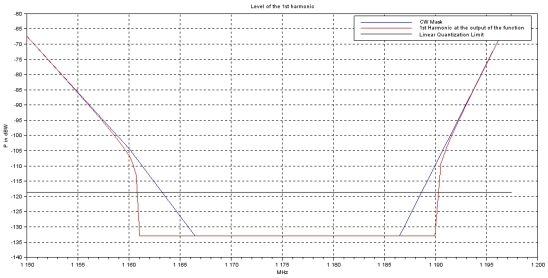

Figure 33. Compression effect of the pure log function on the E5a/L5 CW interference mask

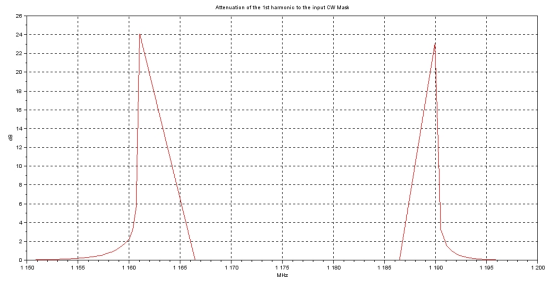

Figure 34. Attenuation provided by the pure log function on the E5a/L5 CW interference mask

The effect of F_{lp} on the CW interference masks was measured as previously for the F_{ll} function. The results are presented in figures 33, 34 and 35 for the E5a/L5 band and in figures 36,37 and 38 for the E1/L1 band.

From the first plots 33 and 36 we can also define the full efficiency band of this function, it is equal to $[1161, 1189]$MHz for E5a/L5 and to $[1553, 1594]$MHz for E1/L1. As expected it is larger than for the linear-then-log function, but slightly. And unfortunately, as in the case of the F_{ll} function, in this full efficiency band the CW interference mask is around or under the linear quantization limit : the CW level to compress is here

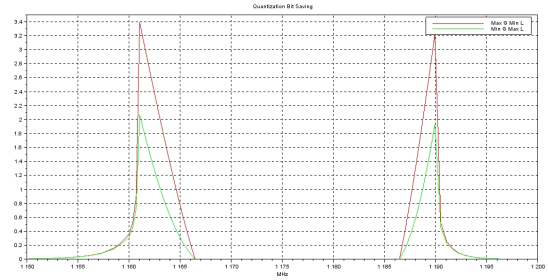

Figure 35. Quantification bit saving offered by the pure log function on the E5a/L5 band

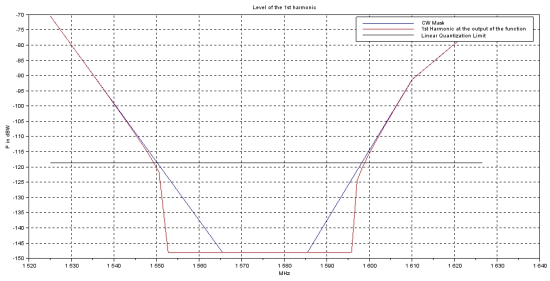

Figure 36. Compression effect of the pure log function on the E1/L1 CW interference mask

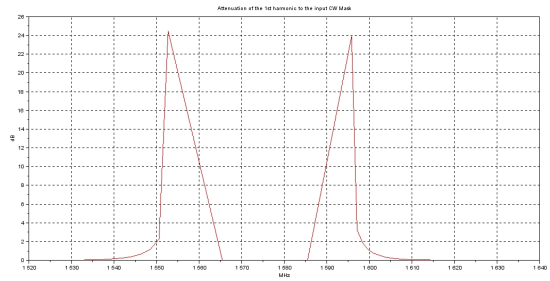

Figure 37. Attenuation provided by the pure log function on the E1/L1 CW interference mask

also the same or smaller than the noise in which the useful signal is buried. We reach the same conclusion than for the F_{pl} function: F_{pl} is efficient where it can not be used.

It is also the conclusion of this part of our study: unless a function with better performance, that is a larger efficiency band, is produced, dynamic compression is not a usable technique to decrease the binary throughput after the ADCs.

6 Band Separation in Coherent Sampling

This last part of the paper is dedicated to the digital separation of the two bands, E5a/L5 and E1/L1, which

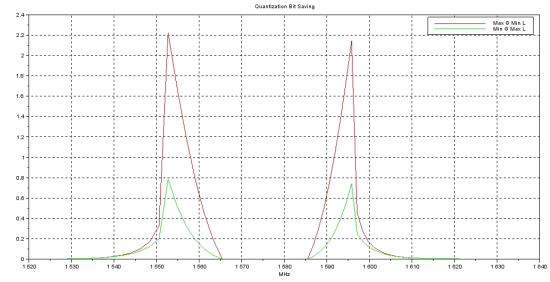

Figure 38. Quantification bit saving offered by the pure log function on the E1/L1 band

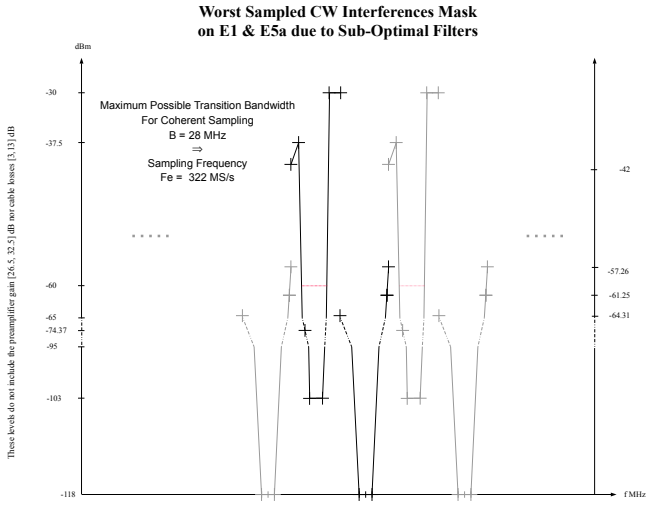

Figure 39. Worst sampled CW interference mask at the output of the ADC in Coherent Sampling

are sampled at the same time in the Coherent Sampling architecture.

The situation to consider at the input of the ADC in structure 6 can be ideal as in figure 8 or as bad as the one represented in figure 16, depending on the selectivity of the analog filters put in front of the ADC. We decide here to study the worst case to bound the complexity of the filters needed to select from one hand the E5a/L5 band and on the other hand the E1/L1 band.

The figure 39 represents the situation of figure 16, aliased in the worst way after sampling at 322.710MSamples/s, which corresponds to the minimum sampling frequency for the maximum transition bandwidth of 28MHz. E5a appears to be the most difficult to separate, from itself, due to the high slope of its interference mask.

The minimum selectivity of the filters mentioned above is drawn in figure 40. The design objective was to allow the greatest decimation rate after the filtering operation. It means that, for each band, after the filter it must be possible to alias the band to itself as near as possible without suffering from an out-band threat reinjected in-band. The attenuation was then calculated so that any out-band level is attenuated to a level of 10dB less than the minimum in-band mask, -103dBm in the E5a/L5 band and -118dBm in the E1/L1 band.

If Finite Impulse Response (FIR) filters are to be used, their order can be estimated using the following formula, from (Kai, 1974)

$$\hat{M} = \frac{-20\log_{10}\left(\sqrt{\delta_p\delta_s}\right) - 13}{14.6\Delta f} + 1 \qquad (3)$$

For the E5a/L5 band it gives $\hat{M} = 1700$ and $\hat{M} =$

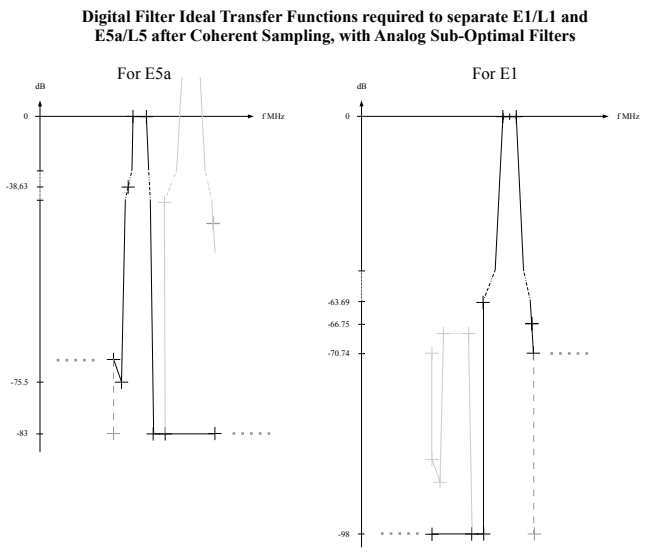

Figure 40. Minimum attenuation to be provided at the output of the ADC, Coherent Sampling

110 for the E1/L1 band. The previous formula, 2 from (Herrmann et al., 1973), was not used here as it is not valid when the ratio $\delta_p/\Delta f$ is less than 0.004 which is the case here. When applicable the formula from (Herrmann et al., 1973) is more accurate but 3 give results of the same order.

The calculation workload can also be estimated here by the simple product of the order $\hat{M}$ and of the sampling frequency. It can reach 548GMAC/s for the E5a/L5 band. This figure should be compared to the performance of the nowadays processors to assess the feasibility of the Coherent Sampling solution with the less selective analog filters. For example the most powerful FPGA from Xilinx, the Virtex-7 XC7V2000T (Xilinx, 2013), which can process up to 5335GMAC/s, seems to offer a sufficient processing power.

7 Conclusion

In summary the paper has reviewed two previously proposed Direct Sampling SDR GNSS receiver architectures designed to take into account the very specific Civil Aviation requirements regarding robustness against interference. On this basis the number of quantification bits required to linearly quantize the input signal has been bounded, from the nominal situation with ideal analog RF filters to the worse situation with low selectivity filters. It appears that an important number of bits is needed to represent the full range of the input signal when interference is present. In view of the important computation workload induced in the following filtering processes, two low complexity non-linear functions have been considered to compress the signal dynamic at the output of ADCs. It has been shown that even if efficient in absolute, these functions are not usable in the proposed architectures. Finally the filters required to digitally separate the E5a/L5 and E1/L1 bands in the Coherent Sampling architecture have been specified and the induced computation workload has been assessed. Future work will focus on the design and implementation of the analog RF filters needed before the ADC(s) in both proposed architectures.

References

(1974). *Nonrecursive Digital Filter Design Using the Io-sinh Window Function.*

(2003). *Design and Practical Implementation of Multifrequency RF Front Ends Using Direct RF Sampling.* ION.

(2011). *Digitization Guidelines for a Direct Sampling Dual-Band GNSS Receiver for Civil Aviation.* European Navigation Conference.

(2012). *Effect of Sampling Jitter on Signal Tracking in a Direct Sampling Dual Band GNSS Receiver for Civil Aviation.* European Navigation Conference.

AD (2006). Analog devices tigersharc adsp-ts201s data sheet.

Alonso, A., Perre, J.-M., and Arizaga, I. (2008). A direct sampling digital receiver for multiple gnss signals. Software Receiver.

EUROCAE (2010). Minimum operational performance specification for airborne open service galileo satellite receiving equipment.

Herrmann, ., Rabiner, . R., and Chan, D. S. K. (1973). Practical design rules for optimum finite impulse response low-pass digital filters. *The Bell System TECHNICAL JOURNAL*, 52(6):769–799.

Parada, E. R., Chastellain, F., Botteron, C., Tawk, Y., and Farine, P.-A. (2009). Design of a gps and galileo multi-frequency front-end.

RTCA (2004). Assessment of radio frequency interference relevant to the gnss l5/e5a frequency band.

RTCA (2006). Minimum operational performance standards for global positioning system / wide area augmentation system airborne equipment.

RTCA (2008a). Assessment of radio frequency interference relevant to the gnss l1 frequency band.

RTCA (2008b). Minimum operational performance standards for gps local area augmentation system airborne equipment.

RTCA (2009). Minimum operational performance standards for global positioning system / aircraft based augmentation system airborne equipment.

Xilinx (2013). 7 series fpgas overview. Advance Product Specification.